Enhanced UV detection by non-polar epitaxial GaN films

Shruti Mukundan, Basanta Roul, Arjun Shetty, et al.

View Online   Export Citation   CrossMark

ARTICLES YOU MAY BE INTERESTED IN

AIP Advances

Mathematical Physics Collection

READ NOW
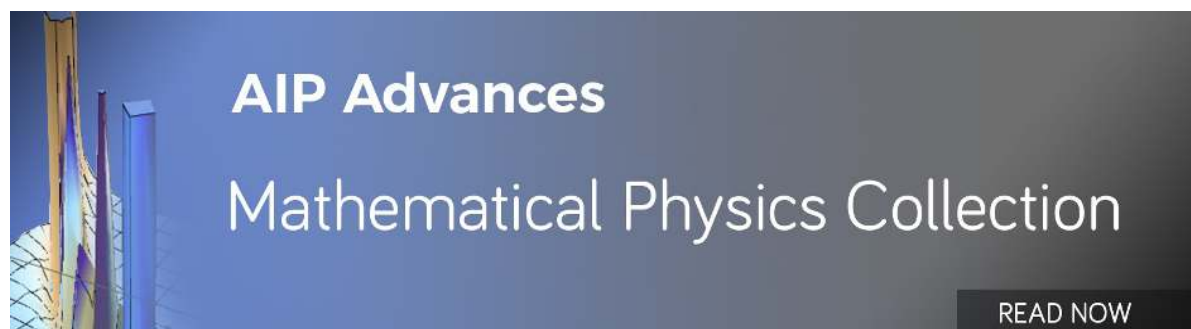
Enhanced UV detection by non-polar epitaxial GaN films

Shruti Mukundan,[1] Basanta Roul,[1,2] Arjun Shetty,[3] Greeshma Chandan,[1] Lokesh Mohan,[1] and S. B. Krupanidhi[1,a]

[1]*Materials Research Centre, Indian Institute of Science, Bangalore, India*
[2]*Central Research Laboratory, Bharat Electronics, Bangalore, India*
[3]*Department of Electrical Communication Engineering, Indian Institute of Science, Bangalore, India*

Nonpolar a-GaN (11-20) epilayers were grown on r-plane (1-102) sapphire substrates using plasma assisted molecular beam epitaxy. High resolution x-ray diffractometer confirmed the orientation of the grown film. Effect of the Ga/N ratio on the morphology and strain of a-GaN epilayers was compared and the best condition was obtained for the nitrogen flow of 1 sccm. Atomic force microscopy was used to analyze the surface morphology while the strain in the film was quantitatively measured using Raman spectroscopy and qualitatively analyzed by reciprocal space mapping technique. UV photo response of a-GaN film was measured after fabricating a metal-semiconductor-metal structure over the film with gold metal. The external quantum efficiency of the photodetectors fabricated in the (0002) polar and (11-20) nonpolar growth directions were compared in terms of responsivity and nonpolar GaN showed the best sensitivity at the cost of comparatively slow response time. © 2015 Author(s). All article content, except where otherwise noted, is licensed under a Creative Commons Attribution 3.0 Unported License. [http://dx.doi.org/10.1063/1.4937742]

I. INTRODUCTION

UV photodetectors have wide range application in industrial, environmental and biological fields.[1,2] Well established Si-based UV detectors with a band gap of 1.1 eV show some significant drawback because of the ageing due to exposure to radiations of much higher energy, resulting in degradation of device performance and increase in dark current. Moreover, the passive layers of SiO_2 reduces the quantum efficiency in the deep UV range.[3] The large and direct band gap of III-nitride materials are proving very advantageous for UV photodetection and a lot of interest to further improve the performance of photodetectors fabricated on III-nitride material is seen in the past few years.[4] First UV photodetector of GaN was reported by Khan et al in 1992.[5] Lack of suitable substrates for the growth of GaN has been a prolong problem and this is a main hindrance in improving the quality of the optoelectronic devices hence fabricated. Improving the crystal quality by suppressing the dislocation densities is seen to reduce noise levels and enhance detectivity of the device.[6] Heterostructures grown along the c-axis exhibit large internal electric fields that affect the radiative recombination rates as well as the carrier transport of the heterostructure barriers.[7] To overcome this polarization issue, there have been concerted efforts in exploring III-Nitride materials and devices along nonpolar and semipolar crystallographic orientations.[8,9]

Different photodetector structures have been explored in the literature such as metal-semiconductor-metal (MSM), Schottky barrier, metal-insulator-semiconductor (MIS), p-n junction and p-i-n junction.[10] Most used photodetectors work in MSM configuration due to their simplicity. The structure consists of two Schottky electrodes deposited on non-intentionally doped semiconductor layer. An external voltage applied between two electrodes biases one of them in forward and another one

[a]Corresponding author. Tel.: 91-80-2360 1330; fax: +91- 80- 2360 7316 E-mail address: sbk@mrc.iisc.ernet.in

in reverse direction. The structure has advantage of very low dark current due to rectifying nature of the contacts, high resistivity of the material, reduced parasitic capacitance, low noise and large internal gain.[11,12] Although, a few reports on nonpolar nanostructures were reported for UV photodetection and it showed promising improvement over the conventional polar orientation, to the best of our knowledge nonpolar oriented GaN epilayers are not yet explored fully for their photodetection efficiencies. Thus, crystallographic orientation and surface polarity is seen to play an important role in deciding the performance of the photodetectors by modifying the metal-semiconductor contact.[13] In this work, we optimized good quality nonpolar (11-20) a-GaN grown on (1-102) r-plane sapphire substrate by changing the growth conditions. The photodetector is fabricated on the best grown film and its performance was compared with photodetector grown on conventional (0 0 0 2) c-plane axis.

II. EXPERIMENTAL

Nonpolar (1 1 -2 0) GaN epilayers were grown on (1 -1 0 2) r-plane sapphire substrates by varying the nitrogen flow. The sapphire substrates were degreased by first boiling in trichloroethylene for 5 minutes and then dipped in acetone and methanol separately for 1 min. The cycle was repeated for 3 times. The substrates were then chemically etched using H_2SO_4:H_3PO_4 (3:1) at 150°C for 20 minutes and rinsed with deionized water before loading into the molecular-beam epitaxy chamber. Thermal cleaning for the substrate was done at 850°C inside the MBE chamber for 30 minutes under ultra-high vacuum (MBE pressure $\sim 1 \times 10^{-10}$ mbar). After nitridation at 700°C for 30 min, GaN films were grown using a two-step processes: i.e., growth of low temperature GaN buffer layer of thickness ~20 nm at 500°C followed by high temperature epilayer of nearly 200 nm grown at 760°C. The Ga effusion cell temperature was kept at 950°C and corresponding beam equivalent pressure (BEP) was maintained at 5.6×10^{-7} mbar. The GaN epilayer growth rate is 70 nm per hour. The nitrogen flow rate was varied from 0.5 sccm (Sample A), 0.75 sccm (Sample B), 1 sccm (Sample C) to 1.25 sccm (Sample D) and the forward RF power of the plasma source was fixed at 350 W. Hence the N/Ga flux ratio was varied for all the samples.

III. RESULTS AND DISCUSSION

2Θ-ω HRXRD scan of nonpolar GaN epilayer oriented in the (1 1 -2 0) direction on (1 -1 0 2) r-plane sapphire (Fig. 1(a)) was confirmed by HRXRD. The peak at 2Θ = 57.7° is assigned to (1 1 -2 0) GaN and at 2Θ = 52.56 is assigned to (2 -2 0 4) Al_2O_3. Figure 1(b) shows the cross sectional SEM image of the (1 1 -2 0) a-GaN epilayer with thickness of around 150 nm for the samples grown for 3 hour. A slight variation in thickness was seen with Ga/N ratio variation but the growth time was modulated to maintain constant thickness for the comparative studies. To compare the surface roughness of all the films, atomic force microscopy was performed. Surface smoothness of the film indirectly indicates the reduction of extended defect densities in the film.[14]

Figure 2 shows the 1×1 μm^2 AFM images for the a-plane GaN films grown at 0.5 sccm, 0.75 sccm, 1 sccm and 1.25 sccm of nitrogen flow respectively. The surface morphology of GaN films was found to depend strongly on the Ga/N flux ratio. The RMS roughness of sample A, B, C and D are found to be 3.05 nm, 2.9 nm, 2.25 nm and 4 nm respectively. Very different mobilities of Ga and N adatoms have important consequences on the growth of GaN.[15] In the Ga rich regime, the Ga adatoms are highly mobile and a step flow mode results in 2D growth. If excess Ga adatoms are present on the surface, N adatoms can be efficiently incorporated since the probability that fast moving Ga adatoms captures N is high. With increase in N flow, we observe much smoother surface morphology. Initially, for very low N flux, the roughness of the surface can be attributed to the excess Ga adatoms in the surface. At the 1 sccm N flux region there is sufficient supply of N for the fast moving Ga adatoms resulting in smooth morphology. Higher N flux pushing the system to N rich condition is expected to result in rougher films.[16]

To quantify the amount of strain present in the film, Raman spectroscopy was used. Fig. 3(a) shows the room temperature Raman spectra of the optimized nonpolar (1 1 -2 0) GaN on r-sapphire grown at 760°C and nitrogen flow of 1 sccm. Raman spectra display A_1 (TO), E_1 (TO) and E_2 (high)
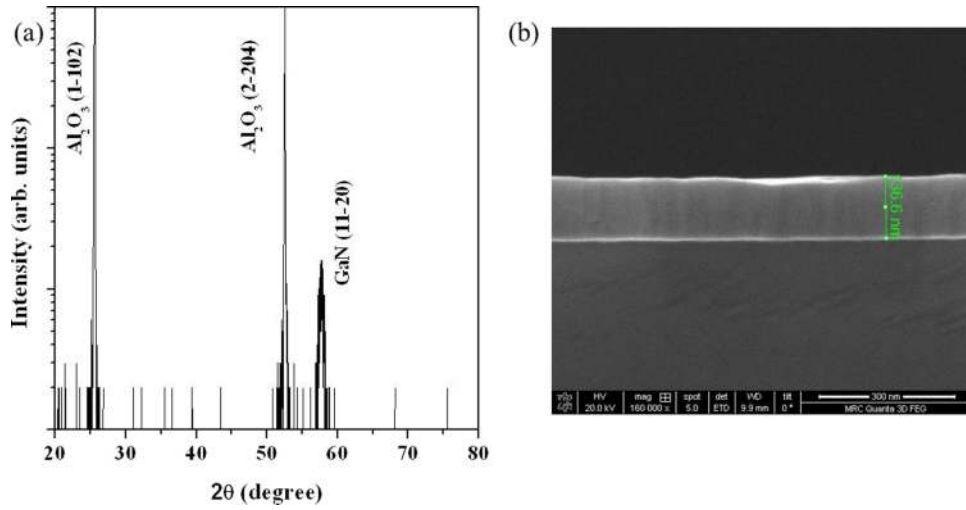
FIG. 1. (a) HRXRD 2Θ-ω scan of nonpolar (11-20) GaN on (1-102) r-plane sapphire (b) Cross sectional FESEM image of a-GaN film on r-sapphire substrate.

phonon mode peaks. The substrate Raman peaks are assigned by asterisk (*). The E_2 (high) phonon mode in the spectra can be used to measure the in-plane strain and the crystalline quality of the film. E_2 mode is sensitive to strain of the GaN crystal and the frequency value of the E_2 mode of strain-free GaN is 568 cm^{-1}.[17] The E_2 (high) peak position for the nonpolar GaN was observed at 569.25 cm^{-1}.
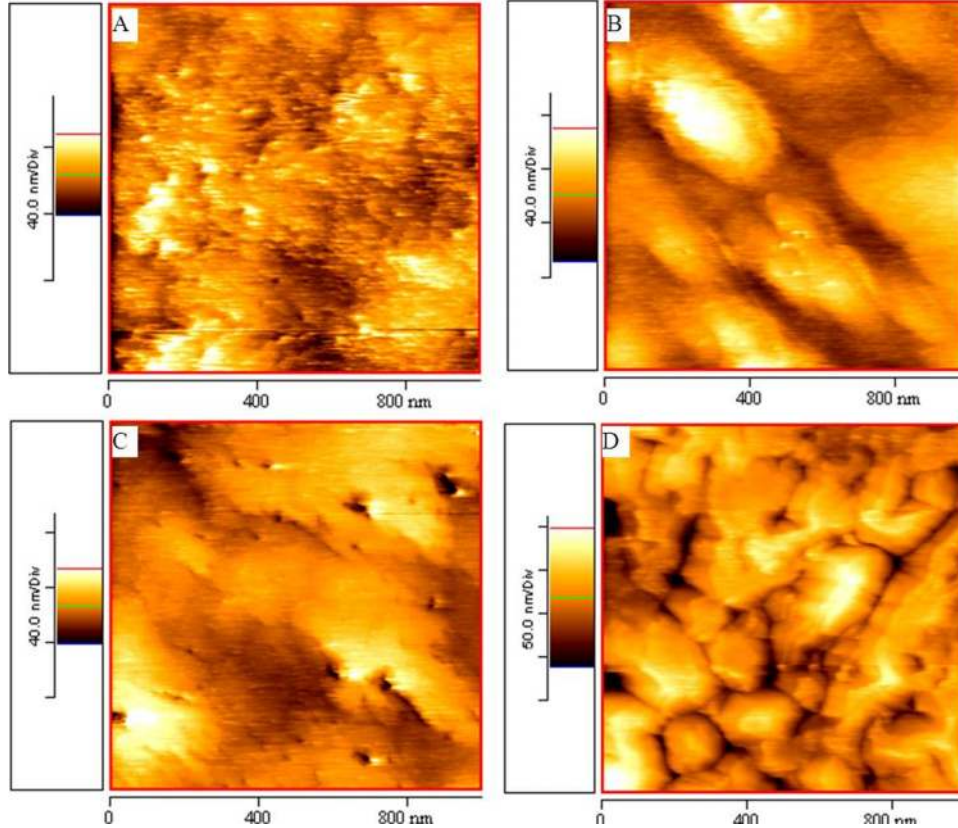

FIG. 2. AFM images for the a-plane GaN films grown at (a) 0.5 sccm, (b) 0.75 sccm, (c) 1 sccm and (d) 1.25 sccm of nitrogen flow.
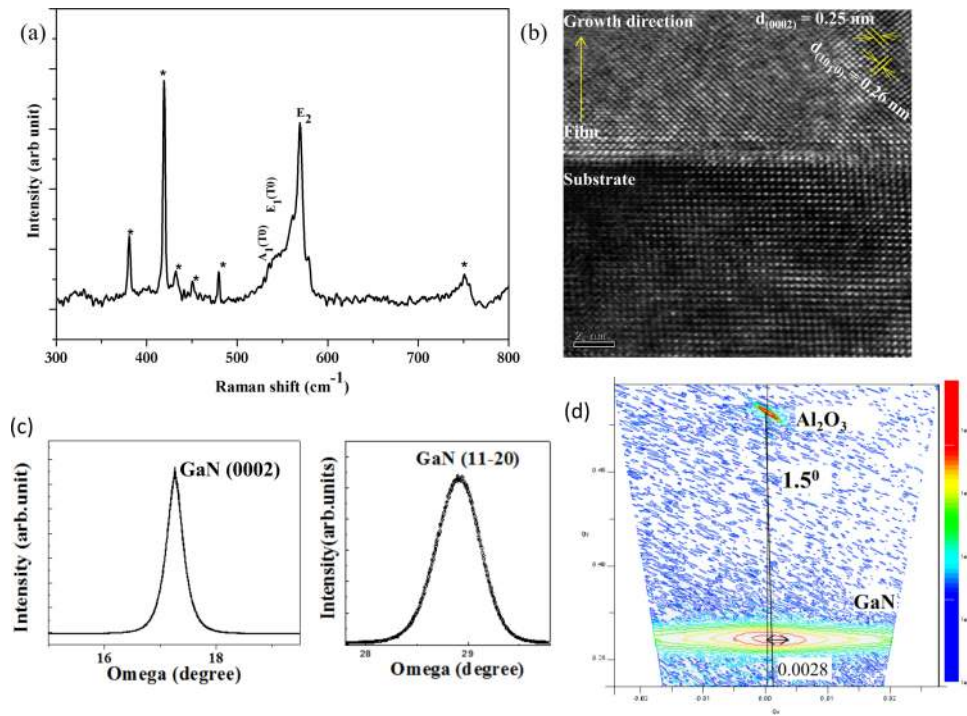
FIG. 3. (a) Raman spectra of the optimized nonpolar (11-20) GaN on r-sapphire substrate (b) HRTEM image of (1 1 -2 0) a-GaN film grown on (1 -1 0 2) r-sapphire substrate (c) Rocking curve of polar c-GaN and nonpolar a-GaN film (d) RSM map of optimized nonpolar (11-20) GaN along the asymmetric (10-10) reflection.

The amount of stress in the sample was calculated by, Eq. (1)

$$\sigma = \Delta\omega/6.2 \text{ GPa} \tag{1}$$

where σ is the biaxial compressive stress expressed in GPa and $\Delta\omega$ is the Raman shift in cm^{-1}.[18] Calculated stress for nonpolar (1 1 -2 0) GaN was found to be -0.02 GPa showing a high value of compressive strain. HRTEM image obtained at the film/substrate interface as shown in Fig. 3(b) shows a very sharp film and substrate interface. High quality interface as seen from the HRTEM image justifies the rigorous optimization steps to achieve highly strained a-GaN with lesser defect densities and high crystallinity.

XRD reciprocal space mapping is one of the core techniques to study the in-plane relaxation state of the film. RSM map along the asymmetric (1 0 -1 0) reflection is conducted under double axis mode on the (1 1 -2 0) a-GaN films and is shown in Fig. 3(d). A 1.5° shift of GaN peak with respect to the substrate position for the film grown at lower nitrogen flow of 1 sccm suggests a very slight relaxation in the epilayer but overall the layer is highly strained. This relaxation affects the crystallinity of the epilayer by increasing the threading dislocation of the system. The lateral spread of the GaN peak along q_x was 0.0028 A^{-1} for the optimized sample which corresponds to very small mosaic spread signifying high crystallinity. The same was confirmed with the AFM analysis and hence this condition was selected as the optimized best condition. Further increase in the nitrogen flow rate affected the mosaic spread and in turn affected the crystalline quality of the sample.

In order to study the UV-photo response of the optimised a-GaN film, photodetector structure was fabricated on the sample by standard photolithography followed by metal (Au) deposition and liftoff to create the interdigited electrode structures with a finger spacing and finger width of 10 μm. Similar device was fabricated on polar c-GaN film to compare its performance with the nonpolar a-GaN. The contacts were annealed in air at 200°C for 15 min. Fig. 4(a) and Fig. 5(a) inset shows the schematic of the device with the gold IDC pattern created on the film.

Fig. 4(a) and Fig. 5(a) show the room temperature I-V characteristics of the nonpolar (1 1 -2 0) GaN and polar (0 0 0 2) GaN in dark and under UV illumination respectively. A lamp of wavelength
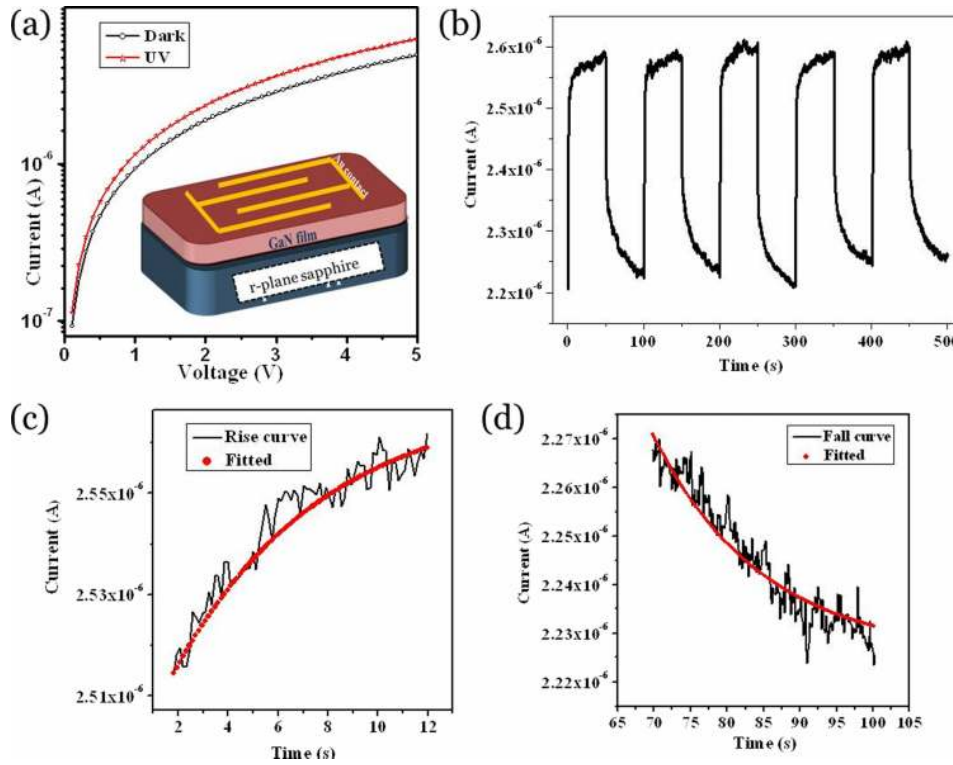
FIG. 4. (a) I-V characteristic of nonpolar a-GaN measured in dark and under UV illumination, (b) the time response of the photocurrent, (c) the time response of the photocurrent for rise time, and (d) the time response of the photocurrent for fall time.

360 nm with intensity 0.3 mW/cm^2 was used as the UV light source for response studies. At 2V applied bias, the dark and photocurrent of the nonpolar a-GaN were 1.9×10^{-6} A and 2.36×10^{-6} A respectively while for the polar c-GaN they were 1.28×10^{-9} A and 1.83×10^{-8} A respectively. Responsivity (R_λ), defined as the ratio of photocurrent generated to the intensity of the incident light on the effective area of a photoconductor, was estimated. External quantum efficiency (EQE) is defined as the number of carriers circulating through a photodetector per absorbed photon and per unit time, and can be expressed as EQE = $hcR_\lambda/e\lambda$ where $R_\lambda = \Delta I_\lambda/P_\lambda S$.[19] Here, ΔI_λ is the difference between the photoexcited current and dark current, P_λ is the light intensity radiated on the sample, λ is the excitation wavelength, S = 0.01 cm^2 is the effective illuminated area for both the devices, h Planck's constant, c the velocity of light and e the electronic charge. EQE is affected by both internal quantum efficiency (IQE) and the light extraction rate. For an incident wavelength of 360 nm at 2V, the measured R_λ was found to be 0.155 A/W for the nonpolar a-GaN and 0.00567 A/W for the polar c-GaN. EQE of the nonpolar a-GaN was found to be 53.3% and that of polar GaN was 0.0195%. These high EQE values are attributed to the high density of defect states at the metal-semiconductor interface of the nonpolar a-GaN.

Fig. 4(b) and Fig. 5(b) shows the measured transit response of the fabricated device at 2 V, as we switched the UV excitation on and off for both the devices. The dynamic response of the device was recorded for 5 on/off cycles and it displayed a rather stable response. With excitation, the photocurrent increased rapidly and then saturated gradually and similar trend was observed while switching off the excitation source. To quantify the response times of the rise and fall of the photocurrent, Eq. (2) and (3) were used,[20]

$$\text{Rise Time}: \quad I(t) = I_{dark} + A\left[1 - \exp\left\{\frac{-(t - t_0)}{\tau}\right\}\right] \tag{2}$$

$$\text{Fall Time}: \quad I(t) = I_{dark} + A\exp\left\{\frac{-(t - t_0)}{\tau}\right\} \tag{3}$$
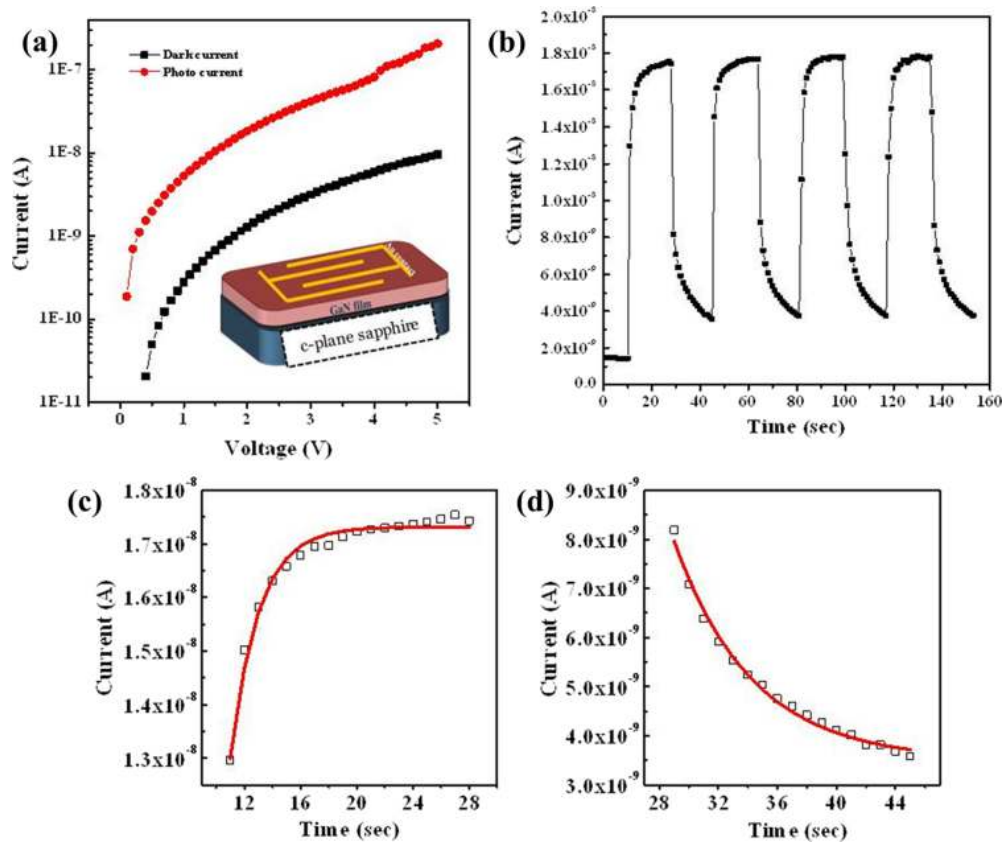
FIG. 5. (a) I-V characteristic of polar c-GaN measured in dark and under UV illumination, (b) the time response of the photocurrent, (c) the time response of the photocurrent for rise time, and (d) the time response of the photocurrent for fall time.

Where I_{dark} is the dark current, A is the scaling constant, τ is the time constant and t_0 is the time when UV light source was switched on or off. The time constant was estimated by fitting Eq. (2) and (3) to the experimental time response of photocurrent during growth and decay as shown in Fig. 4(c) and 4(d) for nonpolar a-GaN and in Fig. 5(c) and 5(d) for polar c-GaN. The value of rise times were found to be 6 s and 2.36 s for nonpolar a-GaN and polar c-GaN respectively while the value of fall times were found to be 15 s and 2.54 s for nonpolar and polar GaN respectively.

Polar c-axis GaN epilayers possess nonpolar m- or a- plane side surfaces while nonpolar a-axis oriented GaN has polar and semipolar sidewalls.[21] Absence of spontaneous polarization in the nonpolar direction results in weaker separation of electron and hole wavefunctions and in efficient recombination of the charge carriers leading to lesser photocurrent.[22] Since the transport of the carriers occurs perpendicular to the growth direction,[23] for the polar c-GaN epilayer, nonpolar sidewalls resulted in lesser photocurrents and hence lower responsivity while in the case of nonpolar a-GaN epilayer with polar and semipolar sidewalls, polarization effect resulted in inefficient recombination and higher photocurrents. The device response and efficiency of the nonpolar a-GaN were found to be higher than that of polar c-GaN. Faster decay time observed in the polar GaN film as compared to the nonpolar one, may account for the lesser defect states formed in the film as the conventionally used polar direction has a higher crystallinity as seen from the FWHM of rocking curve in HRXRD as shown in Fig. 3(c). There has to be a fundamental trade-off between the photoconductive gain and speed of photodetectors because a long minority carrier lifetime will result in an enhancement in photocurrent but increase the response time. In terms of device performance, nonpolar GaN films showed promising results for UV photodetection.

IV. CONCLUSIONS

In summary, we have grown GaN epitaxial films on r-plane sapphire substrates by plasma-assisted molecular beam epitaxy. Nitrogen flux played a significant role in controlling the structural properties of the nonpolar a-GaN films grown on r-sapphire. Orientation of the grown film was confirmed with HRXRD study. Effect of nitrogen flux on the surface morphology of the film showed smoother film at a flow rate of 1 sccm which is an indirect evidence for the reduction of defect levels and hence this condition was chosen as the optimized one. Strain in the epilayer was quantitatively seen in RSM imaging and qualitatively confirmed by Raman spectroscopy. HRTEM revealed high quality interface justifying the good quality epilayer grown. The room temperature UV photodetection was carried out on a-GaN film and the performance was compared with polar c-GaN film. The responsivity and external quantum efficiency of photodetector made with the nonpolar GaN were found to be 0.155 A/W and 53%, respectively while that made with the polar GaN were found to be 0.00567 A/W and 0.0195%. The device response and efficiency of the nonpolar GaN were found to be higher than that of polar GaN. The time response of photocurrent for nonpolar GaN film during rise and fall were found to be 6s and 15s respectively, while that for the polar GaN film were found to be 2.36s and 2.54s respectively. Faster decay time observed in the polar GaN film as compared to the nonpolar one, which may account for the lesser defect states formed in the film, and these observations are consistent with that from the FWHM of the XRD.

ACKNOWLEDGEMENT

[1] P. Fonte *et al.*, Preprint Physics 0502027 (2005).

[2] LE Quintern, Y Furusawa, K Fukutsu, and H Holtschmidt, J Photochem Photobiol B **37**, 158 (1997).

[3] A.M. Suhail, E.K. Hassan, S S Ahmed, and M.K.M Alnoori, Journal of Electron Devices **8**, 268 (2010).

[4] E Munoz, E Monroy, J L Pau, F Calle, F Omnes, and P Gibart, J. Phys.: Condens. Matter **13**, 7115 (2001).

[5] M A Khan, J N Kuznia, D T Olson, J M Van Hove, M Blaingame, and L F Reitz, Appl. Phys. Lett. **60**, 2917 (1992).

[6] K. H. Lee, P. C. Chang, S. J. Chang, Y. C. Wang, C. L. Yu, and S. L. Wu, IEEE Sensors journal **9**(7), (2009).

[7] R. M. Farrell, E. C. Young, F. Wu, S. P. DenBaars, and J. S. Speck, Semicond. Sci. Technol. **27**, 024001 (2012).

[8] P. Waltereit, O. Brandt, A. Trampert, H.T. Grahn, J. Menniger, M. Ramsteiner, M. Reiche, and K.H. Ploog, Nature **406**, 865 (2000).

[9] S. H. Park and D. Ahn, Appl. Phys. Lett. **90**, 013505 (2007).

[10] Liwen Sang, Meiyong Liao, and Masatomo Sumiya, Sensors **13**, 10482 (2013).

[11] Atefeh Habibpoor and Hamid R. Mashayekhi, Journal of Physics: Conference Series **286**, 012035 (2011).

[12] A. Müller, G. Konstantinidis, M. Dragoman, D. Neculoiu, A. Dinescu, M. Androulidaki, M. Kayambaki, A. Stavrinidis, D. Vasilache, C. Buiculescu, I. Petrini, C. Anton, D. Dascalu, and A. Kostopoulos, Applied Optics **47**, 1453 (2008).

[13] R. S. Chen, H. Y. Chen, C. Y. Lu, K. H. Chen, C. P. Chen, L. C. Chen, and Y. J. Yang, Appl. Phys. Lett. **91**, 223106 (2007).

[14] E. A. Fitzgerald, S. B. Samavedam, Y. H. Xie, and L. M. Giovane, J. Vac. Sci. Technol. A **15**(3), (1997).

[15] L. He, X. Gu, J. Xie, F. Yun, A. A. Baski, and H. Morkoç, Mat. Res. Soc. Symp. Proc. **798 Y**, 10.64 (2003).

[16] Yuen-Yee Wong, Edward Yi Chang, Yue-Han Wu, Mantu K. Hudait, Tsung-Hsi Yang, Jet-Rung Chang, Jui-Tai Ku, Wu-Ching Chou, Chiang-Yao Chen, Jer-Shen Maa, and Yueh-Chin Lin, Thin Solid Films **519**, 6208 (2011).

[17] F. Yan, H. Gao, H. Zhang, G. Wang, F. Yang, J. Yan, J. Wang, Y. Zeng, and J. Li, J. Appl. Phys. **101**, 023506 (2007).

[18] T. Kozawa, T. Kachi, H. Kano, H. Nagase, N. Koide, and K. Manabe, J. Appl. Phys. **77**, 4389 (1995).

[19] Linfeng Hu, Jian Yan, Meiyong Liao, Limin Wu, and Xiaosheng Fang, Small. **7**(8), 1012–1017 (2011).

[20] S. Ghosh, B. K. Sarker, A. Chunder, L. Zhai, and S. I. Khondaker, Appl. Phys. Lett. **96**, 163109 (2010).

[21] Xingfu Wang, Yong Zhang, Xinman Chen, Miao He, Chao Liu, Yian Yin, Xianshao Zou, and Shuti Li, Nanoscale **6**, 12009 (2014).

[22] S. Nakamura, Science **281**, 956 (1998).

[23] Aniruddha Konar, Amit Verma, Tian Fang, Pei Zhao, Raj Jana, and Debdeep Jena, Semicond. Sci. Technol. **27**, 024018 (2012).